Inorg. Chem. **2006**, *45*, 4610–4618

Luminescence of Ruthenium Halide Complexes Containing a Hemilabile Phosphine Pyrenyl Ether Ligand

Kristin M. Matkovich,[†] Lisa M. Thorne,[†] Michael O. Wolf,*[,†] Tamara C. S. Pace,[‡] Cornelia Bohne,[‡] and Brian O. Patrick[†]

Department of Chemistry, University of British Columbia, Vancouver, British Columbia, Canada, V6T 1Z1, and Department of Chemistry, University of Victoria, Victoria, British Columbia, Canada, V8W 3V6

Received October 17, 2005

A series of Ru(II) complexes, *tcc*-RuX_2(POC4Pyr-*P*,*O*)$_2$ (X = Cl (**3**), Br (**4**), I (**5**)), containing the hemilabile phosphine pyrenyl ether ligand 4-{2-(diphenylphosphino)phenoxy}butylpyrene (POC4Pyr (**1**)) are reported. The synthesis and spectroscopic properties of both the ligand, POC4pyr (**1**), and ligand oxide, P(=O)OC4pyr (**2**), and the solid-state structure of **1** are reported. Complexes **3**–**5** react rapidly with CO to give complexes *ttt*-$RuX_2(CO)_2$(POC4pyr-*P*)$_2$ (X = Cl (**6**), Br (**7**), I (**8**)). No pyrene excimer emission is detected from **3**–**5**; however, different intensities of excimer emission are observed for **6**–**8**. The intensity of excimer emission decreases through the series, with **6** showing the most intense response. The emission is solely due to intramolecular pyrene excimers at low concentrations ($\leq 10^{-4}$ M). Comparison of the UV–vis and steady-state fluorescence spectra shows overlap between the low energy d–d absorption of **7** and **8** with excimer emission (480 nm), suggesting nonradiative energy transfer may be occurring. Once excess CO is removed, complexes **6**–**8** isomerize to *cis*-dicarbonyl complexes *cct*-$RuX_2(CO)_2$-(POC4Pyr-*P*)$_2$ (X = Cl (**9**), Br (**10**), I (**11**)). The intensity of excimer emission from **9**–**11** increases with respect to the excimer emission observed for **6**–**8**, with **9** showing a significant increase in excimer intensity.

Introduction

Molecule-based sensors, or chemosensors, are molecules that are able to bind selectively and reversibly an analyte of interest with a concomitant change in one or more measurable properties.[1] Optical (absorption or luminescence), electrochemical, magnetic, or mass spectrometric changes may be measured.[2] Special interest has been paid to the development of chemosensors because of their widespread applications in chemistry, biology, biochemistry, cell biology, materials science, and clinical and medicinal sciences.[1]

In the modular design approach to chemosensors, a receptor, reporter mechanism, and spacer are incorporated.[3] The receptor is the site at which the analyte binds, the reporter is where a measurable property change occurs in the presence or absence of analyte, and the spacer joins the receptor and reporter together.[3] A major advantage of this design approach is the ability to rationally adjust properties of the sensor by changing the molecular structure of any of the components.[1]

Luminescence is an attractive reporter mechanism with several advantages including high sensitivity (single molecule detection is possible), quick response time, and direct real-time detection with both spatial and temporal resolution.[3] Furthermore, the properties of the fluorescent lumophores may be tuned to achieve a specific response. To maximize the response, fluorescence should be either ON−OFF or OFF−ON. The quenching of aromatic hydrocarbon fluorescence by transition-metal ions is a well-known phenomenon.[4] In previous work by others, transition-metal complexes were designed and synthesized such that prior to exposure to the analyte, the fluorescence of the fluorophore is quenched by an open-shell transition metal via photoinduced electron transfer (PET) and/or electronic energy transfer (EET) or

* To whom correspondence should be addressed. E-mail: mwolf@chem.ubc.ca.
† University of British Columbia.
‡ University of Victoria.

(1) Prodi, L.; Bolletta, F.; Montalti, M.; Zaccheroni, N. *Coord. Chem. Rev.* **2000**, *205*, 59−83.
(2) Haes, A. J.; Van Duyne, R. P. *J. Am. Chem. Soc.* **2002**, *124*, 10596−10604.
(3) Valeur, B.; Leray, I. *Coord. Chem. Rev.* **2000**, *205*, 3−40.
(4) de Silva, A. P.; Gunaratne, H. Q. N.; Gunnlaugsson, T.; Huxley, A. J. M.; McCoy, C. P.; Rademacher, J. T.; Rice, T. E. *Chem. Rev.* **1997**, *97*, 1515−1566.

10.1021/ic051795j CCC: $33.50
Published on Web 05/18/2006

Scheme 1. Reactivity of *tcc*-RuX_2(POC4Pyr-*P*,*O*)$_2$ toward CO

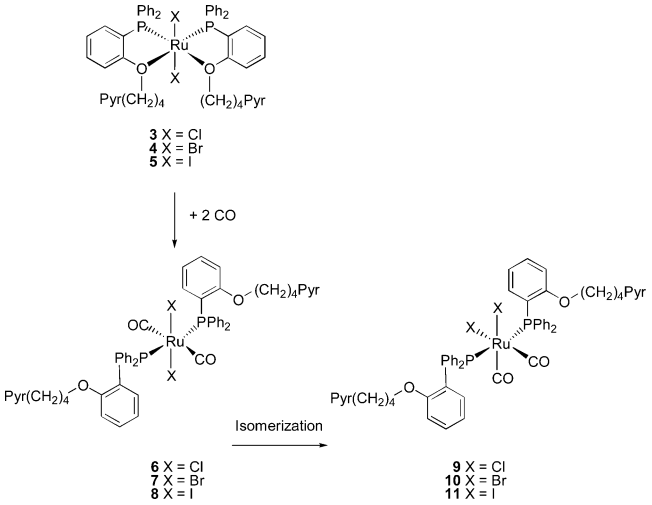

the heavy atom effect.[5−9] Addition of the analyte displaces the fluorescent ligand, or fluorescent moiety of the ligand if the ligand is hemilabile, from the metal center. As a result, ligand fluorescence is revived.

Pyrene is a suitable fluorophore for application in chemosensors because of its well-studied photophysical properties[10−12] and demonstrated ON−OFF functionality via PET and/or EET.[6,13] Sensors based on PET have been developed in which pyrene luminescence is quenched in the presence of open-shell metal ions such as Fe^{3+},[6] Cu^{2+}, and Ni^{2+}.[3] Furthermore, a Zn^{2+} sensor based on an alkyl pyrene group covalently bonded to an aza-18-crown-6 at the nitrogen has been synthesized in which the quenching of pyrene luminescence was shown to depend on the length of the tether between the receptor moiety of the sensor and the pyrene.[13]

In a preliminary communication, we demonstrated that *tcc*-$RuCl_2$(POC4Pyr-*P*,*O*)$_2$ (POC4Pyr = 4-{2-(diphenylphosphino)phenoxy}butylpyrene) (**3**) reacts with CO as shown in Scheme 1.[14] The metal center acts as the receptor via the labile oxygen of the chelating phosphine pyrenyl ether ligand, and luminescent reporting is provided by the pyrene moiety. It was found that CO displaces both of the weakly coordinated ether ligands to form the complex *ttt*-$RuCl_2(CO)_2$-(POC4Pyr-*P*)$_2$ (**6**). The reaction with CO is accompanied by a color change of the solution and the appearance of excimer emission. The initially formed *trans*-dicarbonyl complex

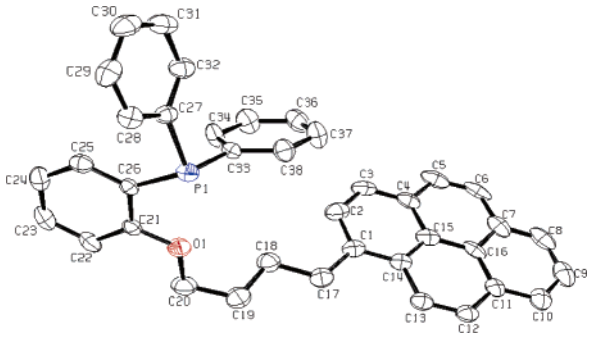

Figure 1. ORTEP view of **1**. The hydrogen atoms are omitted for clarity, and thermal ellipsoids are drawn at 50% probability.

undergoes isomerization after excess CO is removed from solution to form *cct*-$RuCl_2(CO)_2$(POC4Pyr-*P*)$_2$ (**9**).

However, pyrene monomer fluorescence was observed prior to exposure to CO for **3**. One possible way of promoting fluorescence quenching is by altering the energies of the metal d-orbitals through substitution of the chloro ligands for other halides. Herein we report the effect of changing the halide ligand in *tcc*-RuX_2(POC4pyr-P,O)$_2$ (X = Cl (**3**), Br (**4**), I (**5**)) on the luminescence behavior with respect to reaction with CO. The syntheses and characterization of the new compounds, **4** and **5**, their absorption and emission spectra, and their reaction with CO are reported. Differences in the degree of excimer emission between the complexes are discussed. Furthermore, comparison to the phosphine pyrenyl ether ligand POC4pyr (**1**) and the oxidized form of the ligand P(=O)OC4pyr (**2**) provides insight into the type of excimers formed as well as the behavior of the complexes in solution.

Results and Discussion

Synthesis and Characterization of 1 and 2. The synthesis of the phosphine pyrenyl ether ligand **1** was previously reported.[14] Here, the solid-state structure and absorption and emission properties are investigated. The oxide **2** was synthesized by stirring **1** with H_2O_2 in a 1:1 mixture of DCM/acetone. Both **1** and **2** (see Chart 1) were characterized by ^{1}H and ^{31}P{^{1}H} NMR spectroscopies, elemental analysis, mass spectrometry and by UV−vis and fluorescence spectroscopies. Crystals of **1** suitable for X-ray analysis were grown from hot ethyl acetate solution. The solid-state structure is shown in Figure 1. Intermolecular π-stacking is observed in the unit cell between interpenetrating molecules of **1** with a pyrene−pyrene interplanar distance of 3.71 Å. The crystallographic data for **1** are presented in Table 1. The C−X (X = O, P) bond lengths and C−X−C (X = O, P) bond angles (Table 2) closely resemble those reported for (*o*-methoxyphenyl)diphenylphosphine.[15]

The UV−vis absorption spectra of **1** and **2** are essentially identical (Figure 2a,b). The structured absorptions in the UV region arise predominantly from pyrene-based $\pi-\pi^*$ transitions.[10] Weaker absorptions from the rest of the molecule are buried beneath the strong pyrenyl $\pi-\pi^*$ bands.[14] The

(5) Bodenant, B.; Weil, T.; Businelli-Pourcel, M.; Fages, F.; Barbe, B.; Pianet, I.; Laguerre, M. *J. Org. Chem.* **1999**, *64*, 7034−7039.
(6) Bodenant, B.; Fages, F.; Delville, M.-H. *J. Am. Chem. Soc.* **1998**, *120*, 7511−7519.
(7) Wolf, C.; Mei, X. *J. Am. Chem. Soc.* **2003**, *125*, 10651−10658.
(8) Cabell, L. A.; Best, M. D.; Lavigne, J. J.; Schneider, S. E.; Perreault, D. M.; Monahan, M.-K.; Anslyn, E. V. *J. Chem. Soc., Perkin Trans. 2* **2001**, 315−323.
(9) de Silva, A. P.; Fox, D. B.; Huxley, A. J. M.; McClenaghan, N. D.; Roiron, J. *Coord. Chem. Rev.* **1999**, *185*, 297−306.
(10) Birks, J. B. *Photophysics of Aromatic Molecules*. Wiley-Interscience: London, 1970.
(11) Winnik, F. M. *Chem. Rev.* **1993**, *93*, 587−614.
(12) Kalyanasundaram, K.; Thomas, J. K. *J. Am. Chem. Soc.* **1977**, *99*, 2039−2044.
(13) Ji, H.-F.; Dabestani, R.; Brown, G. M.; Hettich, R. L. *Photochem. Photobiol.* **1999**, *69*, 513−516.
(14) Rogers, C. W.; Wolf, M. O. *Angew. Chem., Int. Ed.* **2002**, *41*, 1898−1900.
(15) Suomalainen, P.; Jaaskelainen, S.; Haukka, M.; Laitinen, R. H.; Pursiainen, J.; Pakkanen, T. A. *Eur. J. Inorg. Chem.* **2000**, 2607−2613.

Chart 1

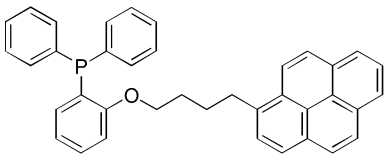

1

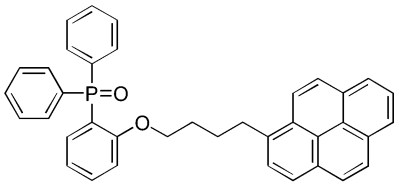

2

Table 1. Crystallographic Data for **1**

chemical formula	$C_{38}H_{31}PO$
fw	534.60
space group	$P2_1/c$ (No. 14)
a (Å)	24.212(3)
b (Å)	15.116(1)
c (Å)	7.6453(7)
α (deg)	90.0
β (deg)	98.276(5)
γ (deg)	90.0
V (Å^3)	2769.0(5)
Z	4
T (°C)	-100.0 ± 0.1
λ(Mo Kα) (Å)	0.71073
D_{calcd} (g cm^{-3})	1.282
μ(Mo Kα) (cm^{-1})	1.30
$R(F_o)^a$ (I > 0.00σ(I))	0.051
$R_w(F_o^2)^b$ (I > 0.00σ(I))	0.103
$R(F_o^2)^a$ (all data)	0.134
$R_w(F_o^2)^b$ (all data)	0.129

^{a} $R = \sum||F_o| - |F_c||/\sum|F_o|$. ^{b} $R_w = (\sum(F_o^2 - F_c^2)^2/\sum w(F_o^2)^2)^{1/2}$.

Table 2. Selected Interatomic Distances and Angles for **1**

	Bond Length (Å)		
O(1)−C(21)	1.364(4)	P(1)−C(27)	1.825(4)
O(1)−C(20)	1.450(4)	P(1)−C(33)	1.824(4)
P(1)−C(26)	1.831(4)		
	Bond Angle (deg)		
C(20)−O(1)−C(21)	116.9(3)	C(26)−P(1)−C(33)	102.45(17)
C(26)−P(1)−C(27)	100.64(18)	C(27)−P(1)−C(33)	102.06(18)
	Torsion Angle (deg)		
P(1)−C(26)−C(21)−O(1)		−6.4(4)	

P_A values, defined as the ratio of the absorption intensity of the ^1L_a band (345 nm) to that of the adjacent minimum at shorter wavelength (337 nm),[11] for **1** and **2** are shown in Table 3. Values of P_A that are less than 3 indicate pyrene preassociation in the ground state, where the degree of preassociation increases the further the value deviates from 3. The P_A values for **1** and **2** are slightly less than 3, indicating a very small amount of preassociation of the pyrene moieties in the ground state. No pyrene excimer emission is observed for concentrations less than 10^{-4} M in the steady-state emission spectra of **1** or **2** (panels c and d of Figure 2), indicating that the small degree of preassociation is not significant enough to influence excimer formation at low concentrations. Excitation of both compounds in dilute solution (10^{-6} M) with UV light leads to indigo-blue emission, as is typically observed for the pyrene monomer.[10] The emission and excitation spectra are near mirror images of each other, and a small Stokes shift typical of fluorescent aromatic molecules is observed.[10] The excitation spectra contain the same features as the absorption spectra. Quantum yields for emission are 0.16 (±0.1) and 0.19 (±0.1) for **1** and **2**, respectively. Single-photon counting (SPC) experiments were carried out, and the lifetimes for **1** and **2** in dichloromethane are 90 ± 5 and 101 ± 2 ns, respectively.

Synthesis and Characterization of Complexes 3−5. The dibromo complex **4** was synthesized using an analogous procedure to that used to prepare **3**,[14] by reaction of ruthenium(III) bromide with **1** in a 5:1 ethanol/toluene mixture. The diiodo complex **5** was synthesized via a halogen exchange reaction of **3** with NaI in acetone. Both complexes were fully characterized by solution methods. No solvent systems were found to yield crystals suitable for X-ray crystallographic analysis. Previously, **3** was fully characterized and its spectral characteristics in solution were compared to those of the complex *tcc*-$RuCl_2$(POMe-*P*,*O*)$_2$ (POMe = 2-methoxyphenyldiphenylphosphine).[14] These assignments were used to aid in the assignment of the structures of **4** and **5**.

One singlet is observed in the $^{31}P\{^1H\}$ NMR spectra of **3**−**5** (Table 3). To confirm the relative stereochemistry of the phosphines, a series of $^{13}C\{^1H\}$ NMR experiments were previously carried out for **3**.[14] Complexes **4** and **5** are presumed to have the same geometry with the two halide ligands *trans*-disposed to one another and the two *P*,*O*-coordinated phosphine ether ligands coordinated such that the phosphines are *cis*-disposed to one another and are chemically equivalent. The similarities in the $^{31}P\{^1H\}$ NMR data for **3**−**5** support this assignment.

The UV−vis absorption spectra of **4** and **5** are essentially identical to that of **3** (Figure 3). Furthermore, the structured absorptions in the UV region of the spectra for **3**−**5** closely resemble those observed for **1** and **2**. Each of the ruthenium complexes also has a weak, metal-based visible absorption band (d−d transition) that gives rise to the observed color (Table 3). The P_A ratios of complexes **3**−**5** (Table 3) are less than those of **1** and **2** indicating that there is more ground-state interaction between the pyrene moieties of **3**−**5**.[11] The molar absorptivities (ϵ_{max}) for the low-energy pyrenyl absorption band vary with halide (**3** < **4** < **5**). This is attributed to changes in the peak breadth, which has previously been related to the degree of ground-state interaction between the pyrene groups.[11]

The emission and excitation spectra for all three complexes are shown in Figure 4. As with **1**, excitation of each complex in dilute solution (10^{-6} M) with UV light gives indigo-blue emission, typical for the pyrene monomer.[10] The emission and excitation spectra resemble those of **1** and **2**, and the excitation spectra are identical to the absorption spectra.

None of the emission spectra for complexes **3**−**5** at any concentration studied ($\leq 10^{-4}$ M) show excimer emission. Pyrene monomer emission is not completely quenched in

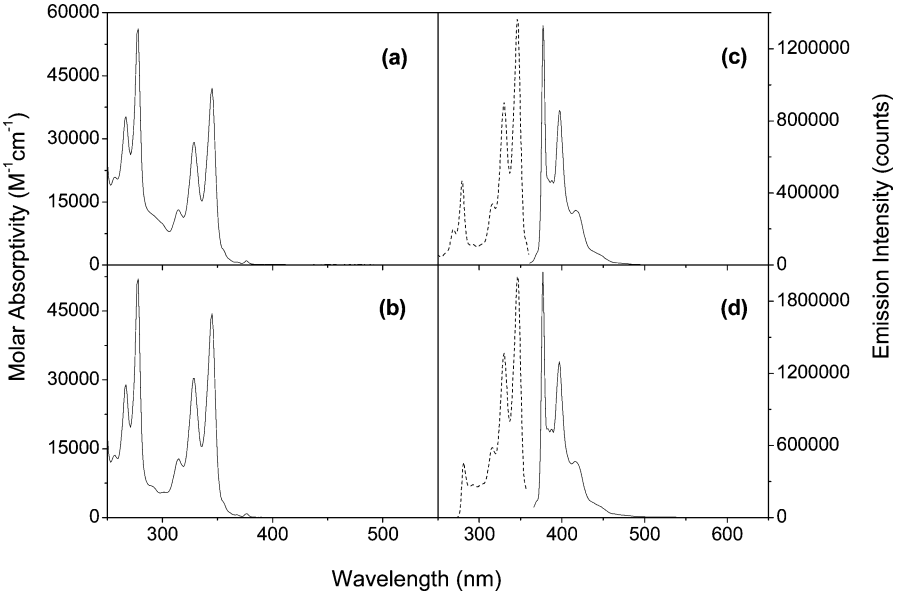

Figure 2. UV−vis absorption spectra for (a) **1** and (b) **2**, [**1**] and [**2**] $\approx 10^{-5}$ M; excitation (- - -) and emission (—) spectra for (c) **1** and (d) **2**, [**1**] and [**2**] $\approx 10^{-6}$ M; $\lambda_{ex} = 345$ nm; $\lambda_{em} = 398$ nm.

Table 3. Summary of Characterization Data for **1**−**11**

compd	$^{31}P\{^1H\}$ NMR δ (ppm)[a]	υ_{CO} (cm^{-1})[b]	λ_{max} (ϵ_{max})[c]	P_A ratio[d]	$\lambda_{(d-d)}$ (ϵ_{d-d})[e]	color
1	−14.2		345 (44 700)	2.8 ± 0.1		colorless
2	27.0		345 (45 000)	2.9 ± 0.1		colorless
3	63.7		345 (61 400)	2.5 ± 0.1	517 (590)	red
4	64.7		345 (71 700)	2.5 ± 0.2	542 (500)	purple−red
5	66.0		345 (89 900)	2.4 ± 0.1	577 (760)	gray−green
6	27.1	2007	345 (61 400)	2.5 ± 0.1	440 (220)	yellow
7	26.0	2001	345 (72 900)	2.3 ± 0.1	455 (250)	light orange
8	22.5	2007	345 (88 300)	2.3 ± 0.1	502 (240)	red−orange
9	13.9	2059, 1998	345 (69 900)	2.5 ± 0.1	none observed	white
10	10.2	2059, 2000	345 (70 700)	2.0 ± 0.1	none observed	yellow
11	5.1	2055, 1989	345 (82 500)	2.2 ± 0.1	shoulder at ∼500	light orange

[a] $CDCl_3$. [b] CH_2Cl_2. [c] λ_{max} (nm) and ϵ_{max} (M^{-1} cm^{-1}) are, respectively, the maximum wavelength and the molar absorptivity of the lowest-energy vibronic band of the ^1L_a electronic transition of the pyrene chromophore (CH_2Cl_2, 25 °C). [d] Determined by averaging P_A ratios from several samples. [e] $\lambda_{(d-d)}$ (nm) and ϵ_{d-d} (M^{-1} cm^{-1}) are respectively the wavelength and molar absorptivity of the metal-based d−d transition (CH_2Cl_2, 25 °C).

any of the complexes. This suggests that either the pyrene moieties are not close enough to the metal center for emission to be quenched, or that the changes in energies of the metal d-orbitals with different halide ligands are not significant enough to lead to quenching of pyrene monomer emission. It has been reported that a tether length of four methylene groups is too long to observe significant quenching of pyrene emission via PET.[13]

When the steady-state emission spectra of **3**−**5** were compared periodically over 48 h, the intensities of the monomer emission increased with time. This suggests some decomposition may be occurring in solution leading to the formation of a more emissive species. The degree of monomer emission increased more quickly for samples stored in light versus those stored in the dark, suggesting a photochemical process is involved. However, samples both stored in the dark and stored in the light showed increases in monomer emission over time suggesting thermal decomposition may also be occurring. No shifts in the emission spectra were observed during this experiment. The formed species was identified by $^{31}P\{^1H\}$ and ^1H NMR spectroscopy as **2**, suggesting that oxidation of some dissociated ligand occurs in solution. It is therefore impossible to exclude the possibility that steady-state emission for **3**−**5** is partially due

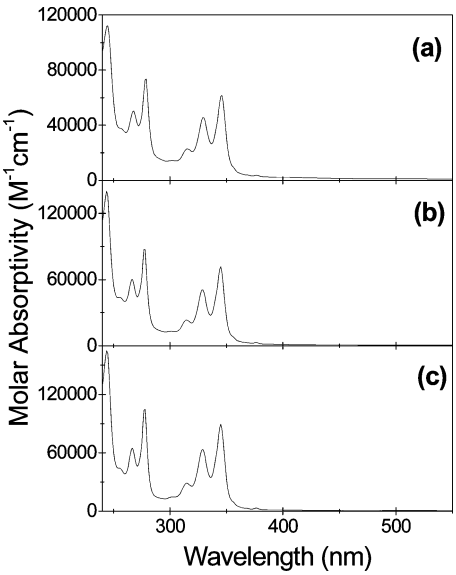

Figure 3. UV−vis absorption spectra of (a) **3**, (b) **4**, and (c) **5**; [*tcc*-RuX_2-(POC4Pyr-*P*,*O*)$_2$] $\approx 10^{-5}$ M.

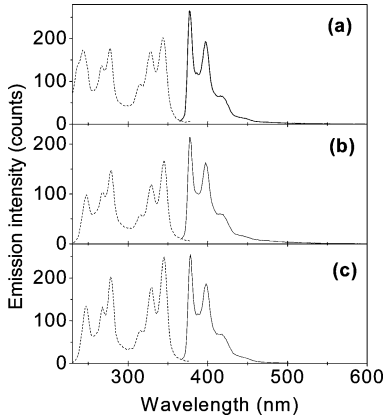

Figure 4. Excitation (- - -) and emission (—) spectra of (a) **3**, (b) **4**, and (c) **5**; [*tcc*-RuX_2(POC4Pyr-*P*,*O*)$_2$] $\approx 10^{-6}$ M; $\lambda_{ex} = 345$ nm; $\lambda_{em} = 398$ nm.

to dissociated ligand (**1**) or ligand oxide (**2**). Thus, neither reliable quantum yield values, nor SPC lifetimes for **3**−**5** could be obtained.

***trans*-Dicarbonyl Complexes 6−8.** It has been shown that complexes of the type RuX_2(POL-*P*,*O*)$_2$ (X = halogen; POL = hemilabile phosphine ether ligand) react with CO to form $RuX_2(CO)_2$(POL-*P*)$_2$ or RuX_2(CO)(POL-*P*,*O*)(POL-*P*).[16−20] Reaction of **3** with CO and accompanying changes in photophysical properties have been described.[14] Complexes **4** and **5** react similarly with CO (Scheme 1), and upon exposure to CO an immediate color change is observed for all three complexes in solution.

A summary of the characterization data for **6**−**8** is shown in Table 3. Reaction of **3**−**5** with CO is accompanied by an immediate shift in the $^{31}P\{^1H\}$ NMR resonance. For all three complexes, the resonances shifted upfield relative to the resonances prior to reaction with CO. Previously, a series of $^{13}C\{^1H\}$ NMR experiments were conducted using ^{13}C-labeled CO to assign the relative stoichiometry of **6** as *ttt*.[14] The stereochemistry of **7** and **8** are assigned in the same way, supported by the similarities in the ^{31}P $\{^1H\}$ NMR chemical shifts and IR bands for the three complexes (Table 3).

The UV−vis absorption spectra of **6**−**8** are essentially identical, with no significant change in the molar absorptivities in the UV region. The absorption bands in the UV region are identical in structure to those of **3**−**5**. The P_A values changed very little relative to those determined for the complexes **3**−**5** (Table 3), supporting a weak interaction between the pyrene moieties of **6**−**8** in the ground state.[11] This is somewhat surprising as the pyrene ligands are disposed differently in **3**−**5** versus in **6**−**8**. For each *trans*-dicarbonyl complex, the weak metal-based transition is blue-shifted relative to its position before exposure to CO (Figure 5). The molar absorptivities of the d−d bands for complexes **6**−**8** are similar to those for complexes **3**−**5** (Table 3).

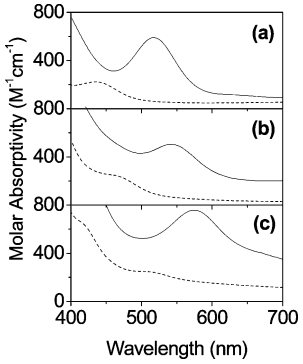

Figure 5. Visible d−d absorption bands of (a) **3** (—) and **6** (- - -), (b) **4** (—) and **7** (- - -), and (c) **5** (—) and **8** (- - -); [*tcc*-RuX_2(POC4Pyr-*P*,*O*)$_2$] and [*ttt*-$Ru(CO)_2X_2$(POC4Pyr-*P*)$_2$] $\approx 2 \times 10^{-3}$ M.

At high concentrations of **3** ($\sim 10^{-2}$ M), reaction with CO under UV irradiation resulted in a change from the weak indigo-blue emission of **3**, characteristic of pyrene monomer emission, to the strong blue-green excimer emission of **6**.[14] This observation is consistent with the formation of intermolecular excimers (Figure 6a).[10] In dilute solution ($\sim 10^{-6}$ M), a small amount of excimer emission was still observed. Since intermolecular excimer formation is insignificant at 10^{-6} M, this must be due to intramolecular excimers (Figure 6b).[10] It was proposed that an increase in conformational freedom of the alkylpyrene moieties occurs after displacement of the ether from the metal center influencing the ability of the pyrene moieties to interact with one another.[14] However, the displacement of the ether moieties from the metal center does not significantly affect the P_A values; that is, it does not influence the ground-state interaction of the pyrene moieties at $\sim 10^{-6}$ M.[11] Thus, the formation of intramolecular excimers appears to be a dynamic process as a result of the increase in conformational freedom.

The intensity of excimer emission from **6**−**8** depends on the nature of the halide ligand (Figure 7). The intensity of excimer emission at 10^{-6} M is lower for **7** and **8** than for **6**; only a very small amount of intramolecular excimer is observed for **7**, and almost no intramolecular excimer is observed for **8**. One possible explanation of this is that the d−d absorption for **7** and **8** is close enough in energy to the pyrene excimer emission, centered at 480 nm, for energy transfer to occur. Since EET is a nonradiative quenching pathway, the extent of excimer emission observed would be expected to be less for **7** and **8** compared to that of **6**. An alternative explanation is that because of the difference in size between the small chloro ligands and the larger bromo and iodo ligands, the alkylpyrene moiety cannot "fold over" the complex as readily to form an intramolecular excimer as shown in Figure 6b. The intensity of excimer emission is limited by the ability of an excimer to form within the lifetime of the excited state of the pyrene monomer[4,11] and by the stabilization of the excimer.[11] Thus, if the lifetimes of the excited states for **7** and **8** are sufficiently shorter than that of **6** such that a conformation suitable for excimer formation cannot be achieved or that the stabilization of the

(16) Gill, D. F.; Mann, B. E.; Shaw, B. L. *J. Chem. Soc., Dalton Trans.* **1973**, 311−317.
(17) Rauchfuss, T. B.; Patino, F. T.; Roundhill, D. M. *Inorg. Chem.* **1975**, *14*, 652−656.
(18) Jeffrey, J. C.; Rauchfuss, T. B. *Inorg. Chem.* **1979**, *18*, 2658−2666.
(19) Krassowski, D. W.; Nelson, J. H.; Brower, K. R.; Hauenstein, D.; Jacobson, R. A. *Inorg. Chem.* **1988**, *27*, 4294−4307.
(20) Lindner, E.; Gepraegs, M.; Gierling, K.; Fawzi, R.; Steimann, M. *Inorg. Chem.* **1995**, *34*, 6106−6117.

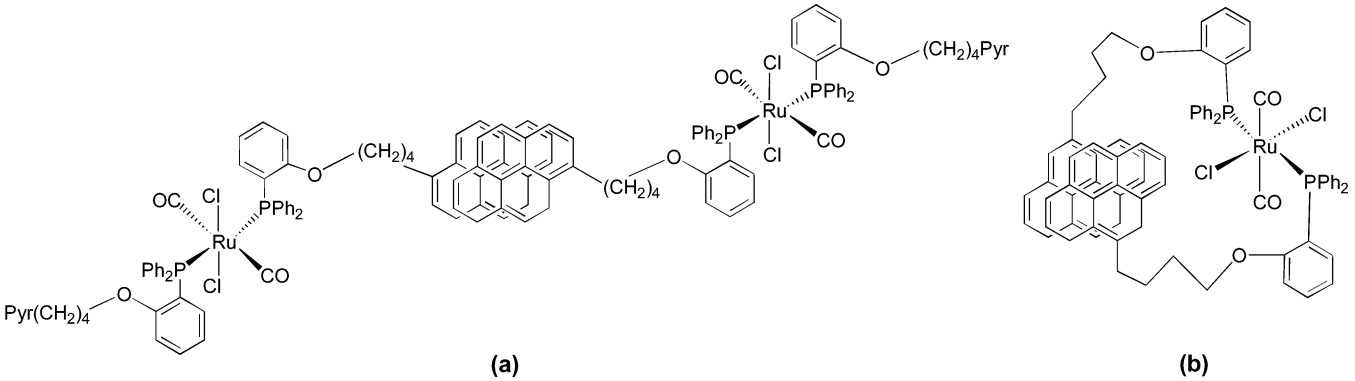

Figure 6. Schematic structure of (a) an intermolecular excimer and (b) an intramolecular excimer for *ttt*-$RuCl_2(CO)_2(POC4Pyr\text{-}P)_2$.

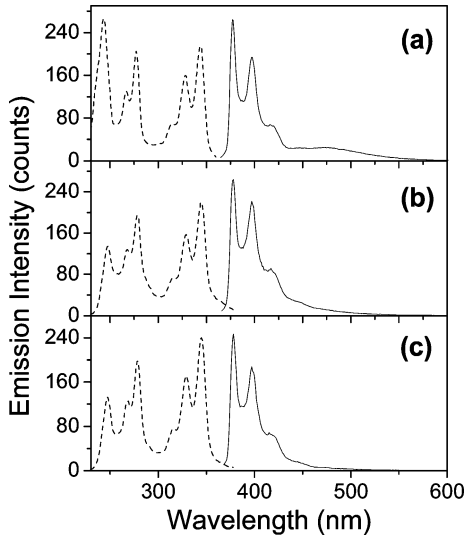

Figure 7. Excitation (- - -) and emission (—) spectra for (a) **6**, (b) **7**, and (c) **8**; [*ttt*-$Ru(CO)_2X_2(POC4Pyr\text{-}P)_2$] $\approx 10^{-6}$ M; $\lambda_{ex} = 345$ nm; $\lambda_{em} = 398$ nm.

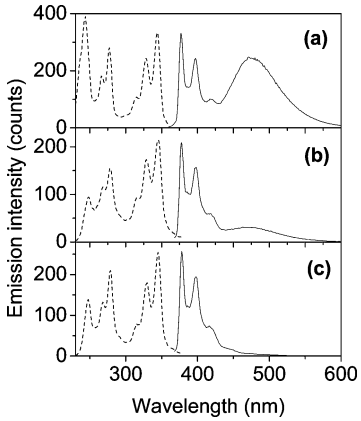

Figure 8. Excitation (- - -) and emission (—) spectra for (a) **9**, (b) **10**, and (c) **11**; [*ccc*-$Ru(CO)_2X_2(POC4Pyr\text{-}P)_2$] $\approx 10^{-6}$ M; $\lambda_{ex} = 345$ nm; $\lambda_{em} = 398$ nm.

excimer cannot overcome the added steric repulsion resulting from the interaction of the alkylpyrene moieties "folding over" the larger bromo and iodo ligands, excimer emission would be significantly reduced or eliminated completely.

***cis*-Dicarbonyl Complexes 9−11.** Complexes of the type *ttt*-$RuX_2(CO)_2(PR_3)_2$ are known to isomerize to the thermodynamically more stable isomers *ccc*-$RuX_2(CO)_2(PR_3)_2$.[19,21] This isomerization typically occurs through a dissociative mechanism.[17] This mechanism is consistent with the observation that isomerization does not occur until excess CO is removed from solutions of **6**−**8** by sparging the solutions with N_2 or by degassing via repeated freeze−pump−thaw cycles (Scheme 1).

A summary of the characterization data for **9**−**11** is given in Table 3. Like the *ttt* isomers, the *ccc* isomers contain two equivalent phosphines, as indicated by the singlet resonance in the $^{31}P\{^1H\}$ NMR spectrum of each complex. The dichloro complex **9** has previously been studied using $^{13}C\{^1H\}$ NMR experiments with ^{13}C-labeled CO to verify the stereochemical assignment as *ccc*.[14] Complexes **10** and **11** are presumed to have the same geometry. Complexes **9**−**11** were also characterized by IR spectroscopy. Two absorptions in the C−O stretching region are expected for *ccc*-$RuX_2(CO)_2(POC4Pyr\text{-}P)_2$; this was observed for all three complexes (Table 3), supporting the assignment of these as *ccc*.

The UV−vis spectra for the *ccc* isomers also show typical absorption from pyrene-based $\pi-\pi^*$ transitions in the UV region.[10] The metal-based d−d transition for **9** and **10** are not observed; they are presumably shifted to higher energy and are obscured by the strong pyrene absorption band. Isomerization of other $RuCl_2(CO)_2(phosphine)_2$ complexes from the *ttt* to the *ccc* isomer results in a color change from yellow to white,[19] consistent with the results observed for **9** and **10**. Complex **11** does show an absorption band at ~500 nm, which appears as a shoulder to the pyrene absorption band, slightly blue-shifted from the absorption of the *ttt* isomer **8**. In addition, the P_A values for each *ccc* isomer are essentially the same as those obtained for the corresponding *ttt* isomer (Table 3), indicating a small degree of pyrene preassociation in the ground state.[11]

Comparison of the fluorescence from the *ttt* isomers **6**−**8** with that from the *ccc* isomers **9**−**11** is interesting. Previously it was reported that strong excimer emission was observed for **9**, even in dilute solution.[14] It was concluded that the pyrene moieties in **9** must be able to more easily interact to form an intramolecular excimer. At 10^{-6} M a small increase in the excimer intensity of **10** is observed with respect to **7** (Figure 8b). Almost no excimer emission is observed for **11** (Figure 8c), similar to the result for complex **8.** These results support the conclusion that intramolecular energy transfer

(21) Bader, A.; Lindner, E. *Coord. Chem. Rev.* **1991**, *108*, 27−110.

may be responsible for the changes in excimer intensity. The blue shift in the d−d band from the *ttt* isomers **6** and **7** to the *cct* isomers **9** and **10** results in poorer overlap between this band and the pyrene excimer, consistent with the increase in excimer intensity for the *cct* isomers of these two complexes. For both **8** and **11**, the d−d band overlaps well with the expected emission band energy from excimer, and in these two complexes no excimer is observed. It is still possible that the larger size of the bromo and iodo ligands impedes the formation of intramolecular excimers, implying that the formation of excimer in **9** is facilitated more easily by the cis disposed chloro ligands rather than by the CO ligands.

Conclusions

The fluorescence of **3**−**5** is very similar because of monomer emission from the pendant pyrenyl groups; after exposure to CO and formation of the *trans*-dicarbonyl product, excimer emission was observed. The dependence of the excimer emission intensity is attributed to differences in the extent of nonradiative energy transfer between the excited-state pyrene moieties and metal-based states in **6**−**8**. Steric constraints may also play a role in favoring excimer formation for **6** over **7** and **8**. There are to our knowledge no other examples in which tuning the electronics at a metal via ancillary ligands results in changes in the intensity of excimer emission from a second ligand. Here, binding with CO triggers the formation of the excimer; however, binding of other ligands in related complexes bearing such hemilabile pyrenyl ligands should also be possible. Fluorescence-based detection of nonfluorescent compounds is thus feasible. Alteration of the ligating end of the hemilabile ligand would allow increased control of binding selectivity and sensitivity. Here, the selected alkyl tether is four carbons long. This length was selected largely on the basis of synthetic accessiblity; however, shorter lengths would clearly be of interest as pyrene emission quenching may be enhanced in these cases. Synthetic approaches to these ligands are being explored.

Experimental Section

General. All reactions were carried out under a nitrogen atmosphere unless otherwise stated. NMR spectra were acquired on either a Bruker AC-200, Bruker Avance 300, or Avance 400 instrument. Residual protonated solvent peaks were used as internal ^{1}H references (vs TMS and δ 0). ^{31}P{^{1}H} NMR spectra were referenced to 85% H_3PO_4 (δ 0). Elemental analyses and mass spectra were both performed by the UBC Department of Chemistry Microanalytical Services Laboratory. Electrospray (ES) mass spectra were obtained on a Micromass LCT time-of-flight (TOF) mass spectrometer equipped with an ES ion source. The samples were analyzed in MeOH/CH_2Cl_2 (1:1) at 100 μM. IR spectroscopic measurements were made using a BOMEM MB155S FTIR spectrometer and using solution samples. All spectra were corrected for solvent by subtracting the appropriate solvent spectrum. UV−vis and fluorescence spectra were all carried out in HPLC grade dichloromethane. UV−vis spectra were obtained using a Cary 5000 UV−vis−near-IR spectrophotometer. A 1-cm quartz cell was used. Fluorescence spectra for **3**−**11** were collected using a Varian Cary Eclipse spectrofluorometer. Measurements were made in a 1-cm quartz cell in air-saturated solutions. For the measurements, 5 nm excitation and emission slit widths were used. Fluorescence spectra for **1** and **2** and quantum yield measurements were obtained on a Photon Technology International fluorimeter using a 1-cm quartz cell. Excitation and emission slit bandwidths were all 4 nm. The quantum yields were determined relative to anthracene. All solutions for quantum yield measurements were sparged with nitrogen gas for a minimum of 10 min. The relative quantum yields in solution were calculated based on the expression[22]

$$\Phi_F = \Phi_F^S \frac{\int_0^\infty I_F(\upsilon)\,d\upsilon}{\int_0^\infty I_F^S(\upsilon)\,d\upsilon}\left(\frac{1-10^{-A^S}}{1-10^{-A}}\right)\left(\frac{\eta}{\eta^S}\right)$$

where Φ_F^S is the quantum yield of the standard, integrals $\int_0^\infty I_F(\upsilon)\,d\upsilon$ and $\int_0^\infty I_F^S(\upsilon)\,d\upsilon$ are the areas under the spectrum of the compound and the standard ($I_F(\upsilon)$and $I_F^S(\upsilon)$ are the intensity of fluorescence of the compound and standard as a function of wavenumber, respectively), A and A^S are the absorptions of the compound and standard, and η and η^S are the refractive indices of the solvent used for the solutions of the compound and standard, respectively.

Time-resolved fluorescence measurements were performed with an Edinburgh Instruments OB 920 single-photon counting system with a hydrogen flash lamp excitation source. The excitation and emission wavelengths were set to 345 and 375 nm, respectively, and the band-pass for the excitation and emission monochromators was ca. 16 nm (2 mm slits). An iris was employed to ensure that the frequency of the stop pulses was smaller than 2% of the start pulse frequency. The number of counts in the channel of maximum intensity was either 10 000 or 2000. A Lauda RM6 bath was used to keep the sample at a constant temperature of 20 °C. The instrument response function is very narrow for the measured time scale (1 μs), and deconvolution of the instrument response function from the decay was therefore not necessary. Data were fitted to monoexponential decays using the Edinburgh software. The value of χ^2 (0.9−1.1) and visual inspection of the residuals and the autocorrelation were used to determine the quality of the fit.[23] Solutions were prepared in dichloromethane by preparing an appropriate 1 mM stock solution and diluting to 1 μM. Solutions were purged with N_2 for at least 20 min prior to measurement.

Chemicals were used as received from the supplier (Aldrich, Strem) unless otherwise specified. Deuterated solvents were used as received from Cambridge Isotope Labs. Carbon monoxide was obtained from Praxair and was used as received. Spectroscopic grade CH_2Cl_2 used for UV−vis and fluorescence measurements gave negligible background luminescence at the excitation wavelengths used for the fluorescence measurements. The synthesis and characterization of POC4Pyr (**1**), *tcc*-$RuCl_2$(POC4Pyr-*P*,*O*)$_2$ (**3**), *ttt*-$RuCl_2(CO)_2$(POC4Pyr-*P*)$_2$ (**6**), and *cct*-$RuCl_2(CO)_2$(POC4Pyr-*P*)$_2$ (**9**) are reported elsewhere.[14]

P(=O)OC4pyr (2). POC4pyr (0.096 g, 0.18 mmol) was dissolved in 20 mL of a 1:1 mixture of dichloromethane and acetone. To the mixture, 30% H_2O_2 (0.05 mL) was added, and the solution was stirred open to air at room temperature for 15 min. The solution was washed with water (3 × 10 mL), and the organic layer was

(22) Kollar, J.; Hrdlovic, P.; Chmela, S.; Sarakha, M.; Guyot, G. *J. Photochem. Photobiol., A: Chem.* **2005**, *171*, 27−38.
(23) Bohne, C.; Redmond, R. W.; Scaiano, J. C. Use of Photophysical Techniques in the Study of Organized Assemblies. In *Photochemistry in Organized & Constrained Media*; Ramamurthy, V., Ed.; VCH Publishers: New York, 1991; pp 79−132.

dried over Na_2SO_4 and concentrated by rotary evaporation to yield a clear, colorless oil. White analytically pure crystals were obtained by drying the oil in vacuo. Yield: 99%. Anal. Calcd for $C_{38}H_{31}PO_2$ (%): C, 82.89; H, 5.67. Found: C, 82.50; H, 6.02. ESI-MS: $m/z = 551$ $(M + H)^+$. $^{31}P\{^1H\}$ NMR (121.4 MHz, 25 °C, $CDCl_3$): δ 27.0 (s). ^1H NMR (200 MHz, 25 °C, $CDCl_3$): δ 8.22−7.90 (m, 9H, pyrene), 7.80 (m, 2H, Ph), 7.70−7.55 (m, 6H, Ph), 7.50 (m, 2H, Ph), 7.15 (m, 2H, Ph), 6.80 (m, 2H, Ph), 4.85 (t, 2H, pyrene-$CH_2(CH_2)_2CH_2$−O), 3.15 (m, 2H, pyrene-$CH_2(CH_2)_2CH_2$−O), 1.65 (t, 2H, pyrene-$CH_2CH_2CH_2CH_2$−O), 1.45 (t, 2H, pyrene-$CH_2CH_2CH_2CH_2$−O); assignments based on previous experiments done for POC4pyr.[14]

***tcc*-RuBr$_2$(POC4Pyr-*P,O*)$_2$ (4).** POC4Pyr (0.382 g, 0.710 mmol) was heated in ethanol (60 mL) to reflux. Toluene (17 mL) was then added to ensure that the ligand was completely dissolved. Distilled water (15 mL) was added to $RuBr_3 \cdot xH_2O$ (0.122 g, 0.360 mmol), and the solution was sonicated for 10 min followed by heating with a heat gun. This treatment was repeated two more times. The ruthenium(III) bromide solution was diluted with an equal volume of ethanol (15 mL) and was then added rapidly to the ligand solution. The reaction was heated at reflux for 72 h. Over the course of the reaction, the solution changed from opaque black to red-purple in color. The reaction mixture was hot-filtered, and the residue was washed with 200 mL of dichloromethane. The filtrate was concentrated to ∼100 mL, by heating the solution to reflux, and then diluted with 200 mL of hexanes. The solution was again heated to reflux and, as the dichloromethane evaporated, a purple-red powder precipitated. This was filtered from the hot solution and washed with hexanes. The red-purple solid was dried in vacuo. Yield: 39%. Anal. Calcd for $C_{76}H_{62}Br_2O_2P_2Ru$ (%): C, 68.63; H, 4.70. Found: C, 68.41; H, 5.00. ESI-MS: $m/z = 1249$ $(M - Br)^+$. $^{31}P\{^1H\}$ NMR (121.4 MHz, 25 °C, $CDCl_3$): δ 64.7 (s). ^1H NMR (200 MHz, 25 °C, $CDCl_3$): δ 8.22−7.85 (m, 16H, pyrene), 7.68 (d, $^3J_{HH} = 8.0$ Hz, 2H, pyrene), 7.38−7.05 (m, 26H, Ph), 6.96 (m, 2H, Ph), 4.78 (m, 4H, pyrene-$CH_2(CH_2)_2CH_2$−O), 3.11 (m, 4H, pyrene-$CH_2(CH_2)_2CH_2$−O), 1.90 (m, 4H, pyrene-$CH_2CH_2CH_2CH_2$−O), 1.67 (m, 4H, pyrene-$CH_2CH_2CH_2CH_2$−O); assignments based on previous experiments done for *tcc*-$RuCl_2$(POC4Pyr-*P,O*)$_2$.[14]

***tcc*-RuI$_2$(POC4Pyr-*P,O*)$_2$ (5).** Acetone (15 mL) was added to *tcc*-$RuCl_2$(POC4Pyr-*P,O*)$_2$ (0.096 g, 0.080 mmol) and NaI (0.054 g, 0.36 mmol). The reaction was heated at reflux for 2 h. During the reaction time, the solution changed from red to green and a green precipitate formed. The reaction mixture was cooled, and acetone was removed in vacuo to give a sticky green solid. The solid was redissolved in dichloromethane and passed through a Büchner funnel to remove NaCl and unreacted NaI. The filtrate was diluted with 100 mL of hexanes. The solution was heated to reflux, and as the dichloromethane was evaporated a green powder precipitated, which was filtered from the hot solution and washed with hexanes. The gray−green solid was dried in vacuo. Yield: 94%. Anal. Calcd for $C_{76}H_{62}I_2O_2P_2Ru$ (%): C, 64.10; H, 4.39. Found: C, 64.06; H, 4.79. ESI-MS: $m/z = 1297$ $(M - I)^+$. $^{31}P\{^1H\}$ NMR (162 MHz, 25 °C, $CDCl_3$): δ 66.6 (s). ^1H NMR (400 MHz, 25 °C, $CDCl_3$): δ 8.11−7.87 (m, 16H, pyrene), 7.69 (d, $^2J_{HH} = 7.3$ Hz, 2H, pyrene), 7.34−7.07 (m, 26H, Ph), 6.96 (m, 2H, Ph), 4.82 (m, 4H, pyrene-$CH_2(CH_2)_2CH_2$−O), 3.16 (m, 4H, pyrene-$CH_2(CH_2)_2CH_2$−O), 2.04 (m, 4H, pyrene-$CH_2CH_2CH_2CH_2$−O), 1.71 (m, 4H, pyrene-$CH_2CH_2CH_2CH_2$−O); assignments based on previous experiments done for *tcc*-$RuCl_2$(POC4Pyr-*P,O*)$_2$.[14]

Reactions with CO. Solutions of **3**, **4**, or **5** in either CH_2Cl_2 or $CHCl_3$ (ranging in concentration from 10^{-1} to 10^{-6} M depending on the experiments being performed) were sparged with CO for a minimum of 5 min after a color change had occurred. The initial *trans*-dicarbonyl product was characterized immediately after exposure to CO. Each solution was sparged with nitrogen in order for the isomerization to occur.

***ttt*-RuBr$_2$(CO)$_2$(POC4Pyr-*P*)$_2$ (7).** Treatment of a red-purple solution of **4** with CO yielded a yellow solution of **7**. IR (CH_2Cl_2): $\nu_{CO} = 2001$ cm^{-1}. $^{31}P\{^1H\}$ NMR (121.4 MHz, 25 °C, $CDCl_3$): δ 26.0 (s). ^1H NMR (200 MHz, 25 °C, $CDCl_3$): δ 8.24−7.58 (m, 26H, pyrene), 7.36−7.12 (overlapping m, 14H), 6.91−6.78 (overlapping m, 6H), 3.94 (m, 4H, pyrene-$CH_2CH_2CH_2CH_2$−O), 3.18 (m, 4H, pyrene-$CH_2CH_2CH_2CH_2$−O), 1.67 (m, 4H, pyrene-$CH_2CH_2CH_2CH_2$−O), 1.40 (m, 4H, pyrene-$CH_2CH_2CH_2CH_2$−O).

***ttt*-RuI$_2$(CO)$_2$(POC4Pyr-*P*)$_2$ (8).** Treatment of a green solution of **5** with CO yielded an orange solution of **8**. IR (CH_2Cl_2): $\nu_{CO} = 2007$ cm^{-1}. $^{31}P\{^1H\}$ NMR (121.4 MHz, 25 °C, $CDCl_3$): δ 22.5 (s). ^1H NMR (200 MHz, 25 °C, $CDCl_3$): δ 8.22−7.64 (m, 26H, pyrene), 7.46−7.03 (overlapping m, 14H), 6.97−6.74 (overlapping m, 6H), 3.87 (m, 4H, pyrene-$CH_2CH_2CH_2CH_2$−O), 3.10 (m, 4H, pyrene-$CH_2CH_2CH_2CH_2$−O), 1.58 (m, 4H, pyrene-$CH_2CH_2CH_2CH_2$−O), 1.41 (m, 4H, pyrene-$CH_2CH_2CH_2CH_2$−O).

***cct*-RuBr$_2$(CO)$_2$(POC4Pyr-*P*)$_2$ (10).** Solutions of **4** treated with CO in CH_2Cl_2 or $CHCl_3$ and degassed with nitrogen after the color change undergo conversion (36 h at room temperature) to the *cis*-dicarbonyl product **10**. IR (CH_2Cl_2): $\nu_{CO} = 2059$, 2000 cm^{-1}. $^{31}P\{^1H\}$ NMR (121.4 MHz, 25 °C, $CDCl_3$): δ 10.2 (s). ^1H NMR (200 MHz, 25 °C, $CDCl_3$): δ 8.22−7.98 (overlapping m, 24H), 7.74−7.58 (overlapping m, 4H), 7.32−7.20 (overlapping m, 14H), 7.12−7.00 (overlapping m, 2H), 6.92−6.80 (overlapping m, 2H), 3.82 (m, 4H, pyrene-$CH_2CH_2CH_2CH_2$−O), 3.16 (m, 4H, pyrene-$CH_2CH_2CH_2CH_2$−O), 1.43 (m, 8H, pyrene-$CH_2CH_2CH_2CH_2$−O).

***cct*-RuI$_2$(CO)$_2$(POC4Pyr-*P*)$_2$ (11).** Solutions of **5** treated with CO in CH_2Cl_2 or $CHCl_3$ and degassed with nitrogen after the color change undergo conversion (36 h at room temperature) to the *cis*-dicarbonyl product **11**. IR (CH_2Cl_2): $\nu_{CO} = 2055$, 1989 cm^{-1}. $^{31}P\{^1H\}$ NMR (121.4 MHz, 25 °C, $CDCl_3$): δ 5.1 (s). ^1H NMR (200 MHz, 25 °C, $CDCl_3$): δ 8.22−7.97 (overlapping m, 24H), 7.76−7.54 (overlapping m, 4H), 7.35−7.15 (overlapping m, 14H), 7.10−6.98 (overlapping m, 2H), 6.92−6.83 (overlapping m, 2H), 3.81 (m, 4H, pyrene-$CH_2CH_2CH_2CH_2$−O), 3.18 (m, 4H, pyrene-$CH_2CH_2CH_2CH_2$−O), 1.50 (m, 8H, pyrene-$CH_2CH_2CH_2CH_2$−O).

X-ray Crystallographic Analyses. A colorless thin-plate crystal of **1** was mounted on a glass fiber, and the data were collected at -100.0 ± 0.1 °C. The structure was solved using direct methods[24] and refined using SHELXTL.[25] All measurements were made on a Bruker X8 APEX diffractometer with graphite monochromated Mo Kα radiation.

The data for **1** were collected to a maximum 2θ value of 45.0°. Data were collected in a series of ϕ and ω scans in 0.50° oscillations with 60.0 s exposures. The crystal to detector distance was 38.02 mm. Data were collected and integrated using the Bruker SAINT[26] software package and were corrected for absorption effects using the multiscan technique (SADABS).[27] The data were corrected for Lorentz and polarization effects. All non-hydrogen atoms were refined anisotropically. All hydrogen atoms were included in calculated positions but not refined.

(24) Altomare, A.; Cascarano, M.; Giacovazzo, C.; Guagliardi, A. *J. Appl. Crystallogr.* **1994**, *26*.
(25) *SHELXTL*, version 5.1; Bruker AXS Inc.: Madision, Wisconsin, 1997.
(26) *SAINT*, version 6.0.2; Bruker AXS Inc.: Madison, Wisconsin, 1999.
(27) *SADABS: Bruker Nonius Area Detector Scaling and Absorption Correction*, version 2.05; Bruker AXS Inc.: Madison, Wisconsin, 2002.

Acknowledgment. The authors thank the Natural Sciences and Engineering Research Council of Canada (NSERC) for funding this work. K.M.M. thanks the UBC Chemistry Department for a graduate fellowship. L.M.T. thanks NSERC and UBC for graduate fellowships. T.C.S.P thanks the University of Victoria for a graduate fellowship.

Supporting Information Available: X-ray crystallography data in cif format for **1** and additional fluorescence spectra for **1**−**5**. This material is available free of charge via the Internet at http://pubs.acs.org.

IC051795J